Raman scattering in pure and Ti-doped $PbHfO_3$ antiferroelectric crystals

1995 J. Phys.: Condens. Matter 7 3957

(http://iopscience.iop.org/0953-8984/7/20/015)

J. Phys.: Condens. Matter 7 (1995) 3957–3972. Printed in the UK

Raman scattering in pure and Ti-doped $PbHfO_3$ antiferroelectric crystals

I Jankowska-Sumara†, G E Kugel‡, K Roleder§ and J Dec§

† Institute of Physics and Computer Science, Cracow Pedagogical University, ulica Podchorazych 2, 30084 Kraków, Poland

‡ CLOES, University of Metz and Supelec, 2 rue Edouard Belin, 57078 Metz Cédex 3, France

§ Institute of Physics, University of Silesia, ulica Uniwersytecka 4, 40007 Katowice, Poland

Received 8 November 1994, in final form 6 February 1995

Abstract. Raman scattering investigations were performed over a large temperature range from 10 to 700 K on pure and Ti-doped $PbHfO_3$ single crystals.

The modifications of the Raman spectra were precisely observed in the vicinity of two structural phase transitions occurring in the crystal: an antiferroelectric (A_1) → antiferroelectric (A_2) phase transition at 436 K and antiferroelectric (A_2) → paraelectric (P) phase transition at 484 K.

The characteristic parameters of the Raman structures were determined throughout the whole phase transition sequence. The softening of the two lowest-frequency Raman lines seems to have a dominating influence on the slight increase in dielectric permittivity at the $A_1 \rightarrow A_2$ phase transition in both pure and doped samples suggesting a displacive nature for this transition.

For Ti-doped samples the form of the $A_1 \rightarrow A_2$ transition is smoother than for undoped samples while the $A_1 \rightarrow P$ transition appears to be unaffected by doping with Ti.

1. Introduction

In recent years the oxides of perovskite structure ABO_3 have been the subject of broad investigations from several points of view (structure and phase transitions, inductive properties, non-linear optical properties, photorefractivity and electrochemical properties). Within this framework the pure and mixed lead-based perovskites of $PbBO_3$ and $Pb(B'_{1-x}B''_x)O_3$ formulae were studied from both the theoretical and the experimental standpoints. Some of these compounds such as $PbTiO_3$ exhibit a wide low-temperature phase of ferroelectric nature. Others are characterized by phases of an antiferroelectric structure below T_c.

$PbZrO_3$ and $PbHfO_3$ are representatives of antiferroelectric crystals. The compounds based on lead zirconate ($PbZrO_3$) have been largely investigated by structural, dielectric, pyroelectric, piezoelectric and electromechanical methods [1–7]. Replacement of Zr by Ti ions markedly influences the $PbZrO_3$ properties and leads to the well known PZT system which is, owing to the excellent electromechanical and memory properties exhibited, particularly interesting for practical applications.

From the dynamic aspect, light scattering and dielectric investigations have been concentrated on $PbZrO_3$ in order to explain the nature and sequence of the phase transition, as well as the large dielectric permittivity values measured at the phase transition, by searching for the soft-phonon-mode behaviour [8, 9] and the relaxation mode [10].

To some extent a similar situation occurs in $PbHfO_3$ for which earlier investigations made on ceramics under air pressure indicated two temperature-induced phase transitions:

0953-8984/95/203957+16$19.50

the first from the paraelectric (P) to the intermediate antiferroelectric (A_2) state and the second to the low-temperature antiferroelectric (A_1) phase [11–14]. While the temperature of the $A_2 \rightarrow P$ transition reported in those papers varied from 477 to 488 K, the $A_1 \rightarrow A_2$ transition was fairly well established at 433–436 K. The P phase exhibits classical cubic perovskite structure $Pm3m$ (O_h^1). The symmetries of the A_1 and A_2 phases have not up to now been finally determined and, according to a suggestion made in [15, 16], they belong to the space group $Pba2$ (C_{2v}^8) or $Pbam$ (D_{2h}^9) for A_1, and one of the symmetries $P222_1$ (D_2^2), $Pmm2$ (C_{2v}^1), $Pmmm$ (D_{2h}^{13}) or $P222$ (D_2^1) for A_2, all of orthorhombic symmetry. The A_1 phase was considered as isomorphous with that of $PbZrO_3$ at room temperature, which was found to be $Pbam$ [17]. Recently, the full three-dimensional *single-crystal* structure of $PbZrO_3$ has been further studied [18]. It was found that this structure is disordered in the oxygen sublattice and also described as the centrosymmetric $Pbam$.

According to the Lyddane–Sachs–Teller relation, the large dielectric permittivity divergence observed near the ferroelectric or antiferroelectric phase transitions should be associated with the softening of low-frequency transverse optical (TO) phonon modes. For the ferroelectrics $BaTiO_3$ and $PbTiO_3$, the share of the soft mode in the ϵ'-value at T_c is incomparably weaker than that from the low-frequency mode of relaxational nature [19, 20]. For antiferroelectric materials the problem is not well recognized. To the best of our knowledge there is virtually no reported information on lattice dynamics in lead hafnate which undergoes two different antiferroelectric phase transformations. Hence, it was decided to undertake systematic Raman spectroscopy investigations of this compound with the aim of measuring the light scattering spectra of pure $PbHfO_3$ (PH) and of a $PbHfO_3$ single crystal doped with a small amount of $PbTiO_3$ i.e. $PbHf_{1-x}Ti_2O_3$ (PHT), and comparing the results with dielectric and structural investigations.

2. Experimental results

2.1. Crystal growth and dielectric measurements

Our investigations were performed on two kinds of crystal grown by the flux method. A mixture of $PbHfO_3$ (and $PbTiO_3$ in the case of PHT), PbO and B_2O_3 was used and the growth process was carried out from 1473 to 1223 K with a cooling rate of 12 K h^{-1}. Transparent yellow crystals of rectangular shape and polydomain structure were obtained and used in both the dielectric and the Raman scattering measurements. For the doped sample, the concentration x equal to 4.02% was established by x-ray microanalysis investigations.

Variations with temperature in the dielectric susceptibility on cooling and heating were measured on a 1 MHz automatic capacitance bridge. The $\epsilon'(T)$-dependences for both PH and PHT are shown in figure 1. The results are basically similar to those quoted for PH in the literature; a small but clear additional anomaly close to $P \leftrightarrow A_2$ was found (its origin is not yet known). For the PHT sample, dielectric measurements evidence a shift in the transient A_2 phase towards lower temperatures and a smoother form of the $\epsilon'(T)$ curve through the $A_2 \leftrightarrow A_1$ transition in comparison with pure PH. The $P \leftrightarrow A_2$ phase transition seems to be independent of Ti doping and takes place at 484 K with a sharp divergence in ϵ' and only a very small thermal hysteresis (about 0.5 K).

2.2. Raman scattering measurements and results

2.2.1. Experimental conditions and vibrational modes. The Raman scattering experiments were performed using a Spex double monochromator with the 6328 Å He–Ne laser line

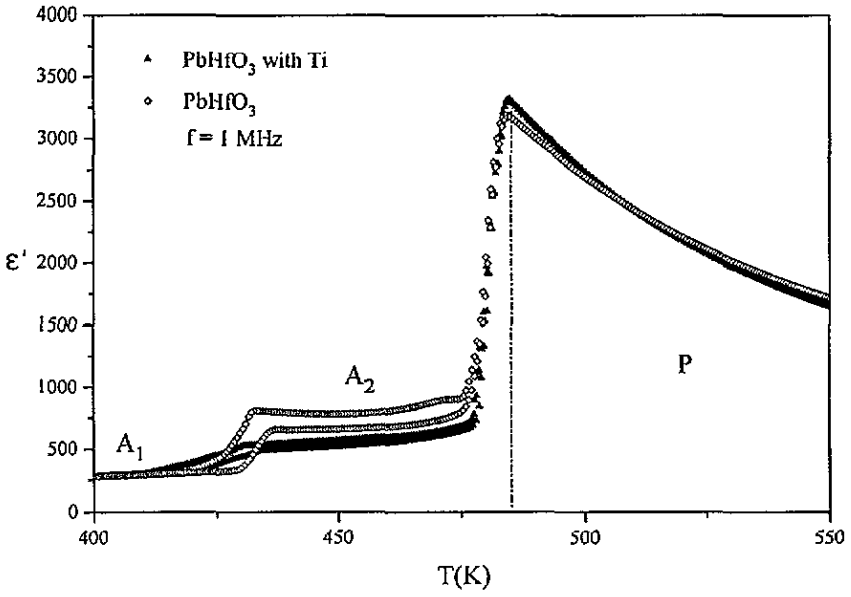

Figure 1. Temperature dependence of the dielectric constant measured at 1 MHz for pure $PbHfO_3$ (PH) and Ti-doped $PbHfO_3$ (PHT). (On heating (upper lines) and on cooling (bottom lines).)

in a temperature range from 10 to 700 K. For measurements above room temperature, the sample was put into a temperature-controlled furnace. The low-temperature spectra were measured in an Air-Product Displex cryostat with an automatic temperature controller.

In a symmetry analysis of the vibrational modes, the symmetry of the intermediate antiferroelectric A_2 phase is not finally defined. Of the possible space groups to which the system could belong the most probable are assumed to be $Pmm2$ (C_{2v}^1) and $P222_1$ (D_2^2) or $P222$ (D_2^1). The space group denoted $Pmmm$ (D_{2h}^{13}) was excluded on the basis of the subgroup sequence. Because the space groups $P222_1$ (D_2^2) and $P222$ (D_2^1) are described by the same number of vibrational modes and the same kinds of vibrational mode, we can simplify our considerations into the two most probable (C_{2v}^1 and D_2^2). In both cases, the vibrational modes are Raman active and their number should be equal to 120, unlike the low-temperature A_1 phase in which only 48 modes are active. Hence, the structural phase transition should be characterized by activation (on heating) of previously Raman-silent phonon modes.

The theoretical group analysis of the vibrational modes in $PbHfO_3$ in the three phases A_1, A_2 and P using two assumptions of the A_2 phase is reported in table 1.

2.2.2. Raman results for $PbHfO_3$. A comparison of Raman spectra recorded in the usual frequency range from 0 to 800 cm^{-1} at 10 K and at room temperature is given in figure 2. In both cases the low-frequency (0–200 cm^{-1}) range is presented in more detail (see inset). The spectra obtained at 10 K exhibits about 40 structures of various intensities which means that the majority of the Raman-active modes are seen. Exact symmetry indexation was, however, impossible because of the polydomain character of the sample. Heating from 10 K to room temperature leads to Raman spectra in which the peaks exhibit a normal increase in damping, a shift in the frequency but no drastic change in the spectrum, indicating the absence of

Table 1. Theoretical group analysis of the vibrational modes for $PbHfO_3$ single crystal.

Phase	Paraelectric	Antiferroelectric		Antiferroelectric
Symbol	P	A_2		A_1
Space group	$Pm3m$ (O_h^1)	$Pmm2$ (C_{2v}^1)	$P222_1$ (D_2^2)	$Pbam$ (D_{2h}^9)
Symmetry	Cubic	Orthorhombic	Orthorhombic	Orthorhombic
Number z of $PbHfO_3$ in the unit cell	1	8	8	8
Number of vibrational modes	15	120	120	120
Symmetry decomposition of vibrational modes	$4F_{1u} + F_{2u}$	$36A_1 + 12A_2 + 36B_1 + 36B_2$	$20A + 28B_1 + 36B_2 + 36B_3$	$16A_g + 8B_{1g} + 12B_{2g} + 12B_{3g} + 4A_{1u} + 20B_{1u} + 24B_{2u} + 24B_{3u}$
Raman-active modes	0	$36A_1 + 12A_2 + 36B_1 + 36B_2$	$20A + 28B_1 + 36B_2 + 36B_3$	$16A_g + 8B_{1g} + 12B_{2g} + 12B_{3g}$

any transition between 10 and 300 K. Since the clearest part of the spectrum appears in the frequency part lower than 200 cm^{-1}, description of the temperature-dependent Raman spectrum will be undertaken in this range only on the basis of Raman lines a, b, c, d, e, f and g as labelled in figure 2.

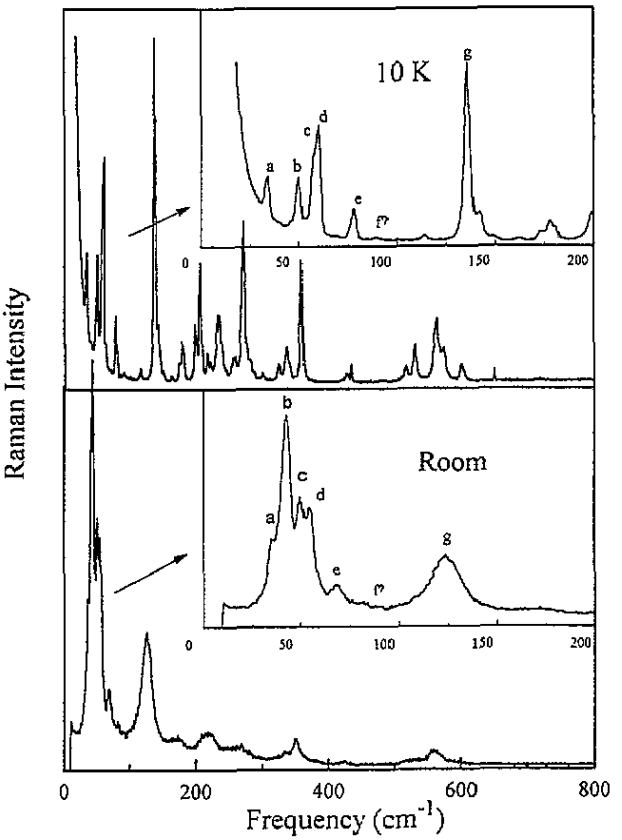

Figure 2. Raman spectra recorded for pure PH at 10 K and at room temperature.

Figure 3 presents Raman spectra recorded near the $A_1 \rightarrow A_2$ transition which are typical of the A_1 phase (434 K) and A_2 phase (441 K) as well as of the transition range at 438 K.

The main modifications through the transition are as follows:

(i) a shift downward in the low-frequency a and b lines with simultaneous increase in low-frequency scattering (see arrow);

(ii) disappearance of the shoulders d and e and the formation of one main band;

(iii) strong activation of a mode at about 85 cm^{-1} (called f);

(iv) clear softening of the g line.

In agreement with the behaviour of the dielectric permittivity (figure 1), the transition $A_1 \leftrightarrow A_2$ occurs in a wider temperature range.

The phase transition from the intermediate A_2 phase to the cubic P phase is given in figure 4 and shows an abrupt disappearance of the Raman structures. The P phase

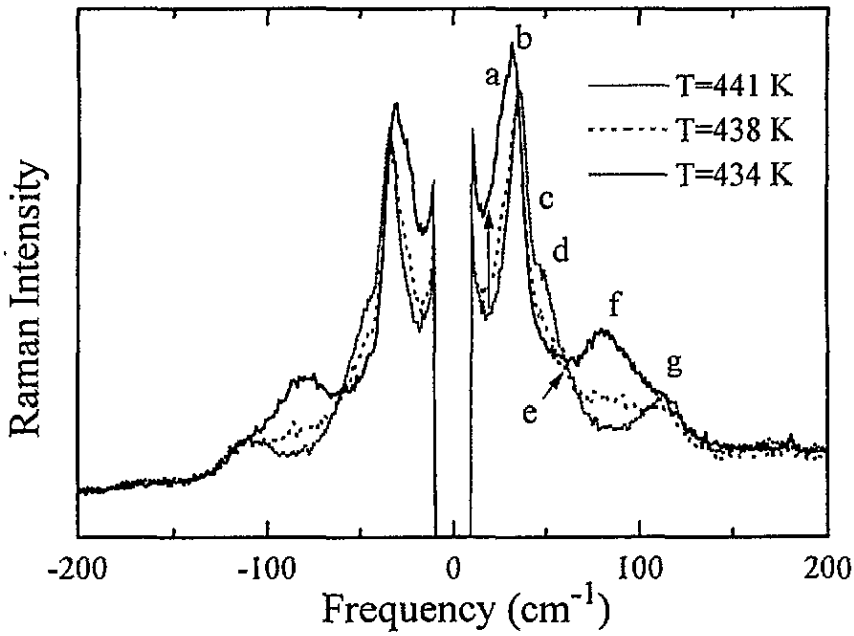

Figure 3. Raman spectra recorded on heating for pure PH below (434 K), near (438 K) and above (441 K) the phase transition $A_1 \rightarrow A_2$.

is characterized by the persistence of strong quasi-elastic scattering and a temperature-dependent low-frequency bump. The temperature dependence of this spectrum will be shown and analysed in section 3.4.

It is also noteworthy that the modifications in Raman spectra through the $A_1 \leftrightarrow A_2$ and $A_2 \leftrightarrow P$ transitions on heating and cooling are in excellent agreement with the hysteresis phenomenon seen in the dielectric response.

2.2.3. Case of $PbHf_{1-x}Ti_xO_3$. Comparison of the PHT spectra with those obtained for PH indicates that a small addition of Ti ions does not significantly modify the shape and number of Raman lines in the A_1, A_2 and P phases. The most significant change is connected with the broader temperature range of the $A_1 \rightarrow A_2$ transformation and the decrease in its temperature. For illustration, the temperature evolution of the Raman spectra in the vicinity of the $A_1 \rightarrow A_2$ phase transition in PHT is presented in figure 5.

3. Analysis and discussion of experimental results

3.1. Analysis of the Raman spectra

In order to achieve an accurate description of the light scattering spectra, the Raman intensities have been systematically fitted with a scattering response function including two kinds of contribution:

$$I_t(\omega) = K\left(\sum_i I_{0i}(\omega) + I_R(\omega)\right) \tag{1}$$

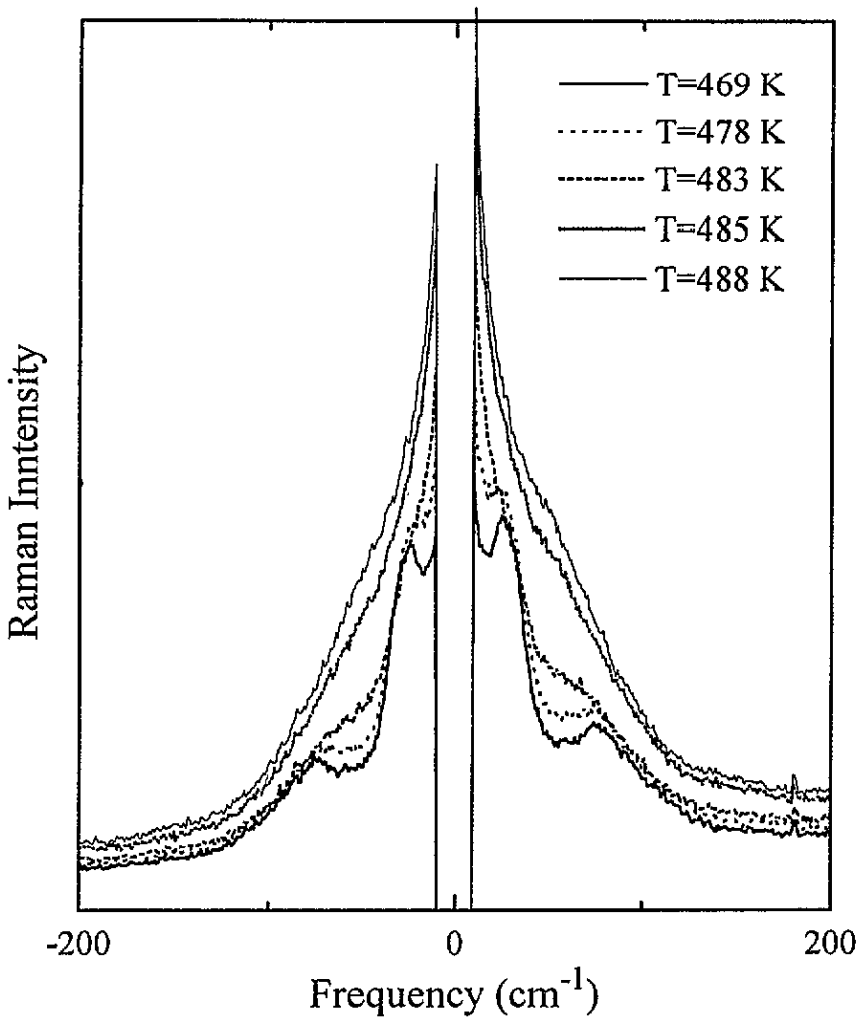

Figure 4. Raman spectra recorded in the heating process for pure PH through the $A_2 \rightarrow P$ transition ($T_{A_2-P} = 484$ K).

where $I_{0i}(\omega)$ is a Lorentzian-like function for the phonon mode oscillators which is written for each individual oscillator:

$$I_{0i}(\omega) = \frac{n(\omega)+1)}{n(\omega)} \frac{S_i \omega_i^2 \gamma_i \omega}{(\omega_i^2 - \omega^2) + \gamma_i^2 \omega^2} \tag{2}$$

and $I_R(\omega)$ is a Debye-like function for the quasi-elastic scattering originating from relaxational motion:

$$I_R(\omega) = \frac{n(\omega)+1}{n(\omega)} \frac{\omega S_r \gamma_r}{\omega^2 + \gamma_r^2}. \tag{3}$$

The factors $n(\omega)$ and $n(\omega) + 1$ are the so-called Bose–Einstein factors and correspond to anti-Stokes and Stokes scattering, respectively. K is a coefficient which depends on

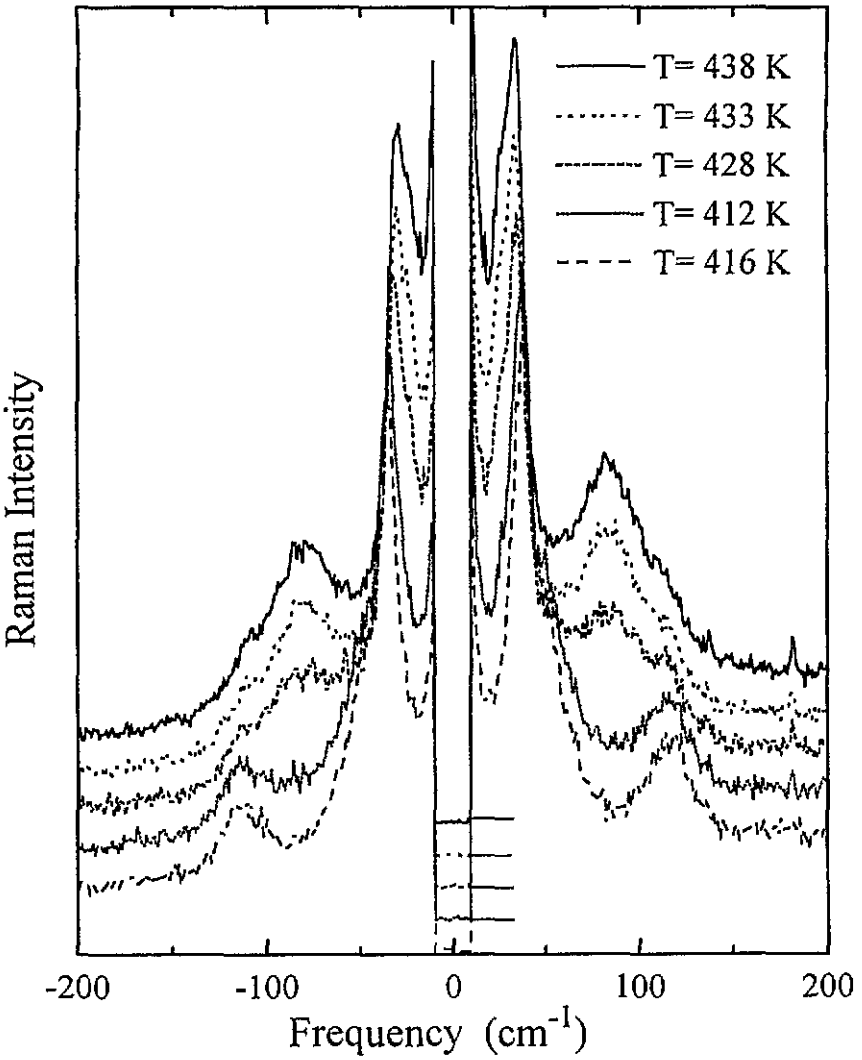

Figure 5. The evolution of low-frequency Raman spectra for PHT between the A_1 and A_2 phases (on heating).

experimental conditions. S_r and γ_r describe the strength and relaxation rate, respectively, of the relaxor. The light scattering due to the so-called damped oscillator is characterized by the strength S_i, frequency ω_i and damping γ_i. A typical example of the fit performed for our Raman measurements is presented in figure 6.

Figure 7 shows the temperature dependence of the frequencies of the Raman lines a–g from 10 K to the $A_2 \rightarrow P$ transition. The inset shows more clearly the $A_1 \rightarrow A_2$ phase transition. Our calculations indicate a softening of the two lowest lines a and b on approaching $T_{A_1-A_2}$. Above this temperature these modes stabilize. The line g, showing continuous deccrease with increasing frequency without any singularity at $T_{A_1-A_2}$, unlike the lines a and b, is not connected with this transition. As mentioned in the symmetry considerations, the appearance of the line f can be attributed to the activation of previously silent Raman modes. No activation of other modes could be detected. This is mainly because

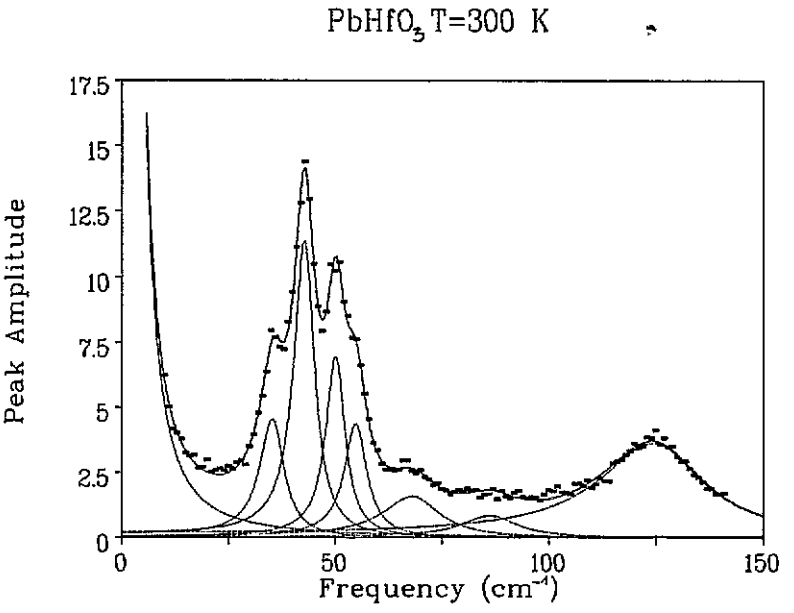

Figure 6. Typical example of quantitative treatment of a low-frequency Raman spectrum.

at these temperatures the main parts of the vibrational modes are difficult to observe, because of their small scattering strength and marked dampiing.

The scattering strength intensity S_r for the relaxational mode obtained in our calculations is presented in figure 8. This strength increases as the temperature approaches T_{A_2-P}, without any singularity at the $A_1 \rightarrow A_2$ transition. This indicates that the $A_1 \rightarrow A_2$ transition seems to be of a displacive nature and is not influenced by a relaxation process. The $A_2 \rightarrow P$ transition will be considered separately.

Figure 9 shows the changes in integrated intensity and damping parameter γ_i for those Raman lines detected, i.e. a, b and f, which play the most important role at the $A_1 \rightarrow A_2$ transition. Of particular importance is the line a (figure 9(a)) exhibiting marked changes in the parameter γ_i which causes experimentally observed quasi-elastic scattering. Clear activation of the line f at the $A_1 \rightarrow A_2$ transition can be seen in figure 9(c).

3.2. Raman spectra for PHT

Similar calculations were systematically performed for the PHT sample. Results of the line frequencies in the vicinity of the $A_1 \rightarrow A_2$ and $A_2 \rightarrow P$ phase transitions are shown in figure 10. The broken lines corresponding to the equivalent frequencies in the pure PH samples are added for comparison, making it possible to distinguish the modes which indicate motion involving Ti(Hf) ions. This appears to be the case for the lines a, b, f and g which exhibit, as would be expected, an increase in mode frequency after the introduction of Ti.

3.3. Dielectric calculations in the vicinity of the A_1 and A_2 phase for PH and PHT

As mentioned in section 2.1 (figure 1), the $A_1 \rightarrow A_2$ transition is accompanied by a significant jump in the low-frequency dielectric constant when going from A_1 ($\epsilon \simeq 250$) to A_2 ($\epsilon \simeq 600$). Since the two phases involved in this phase transition are both known

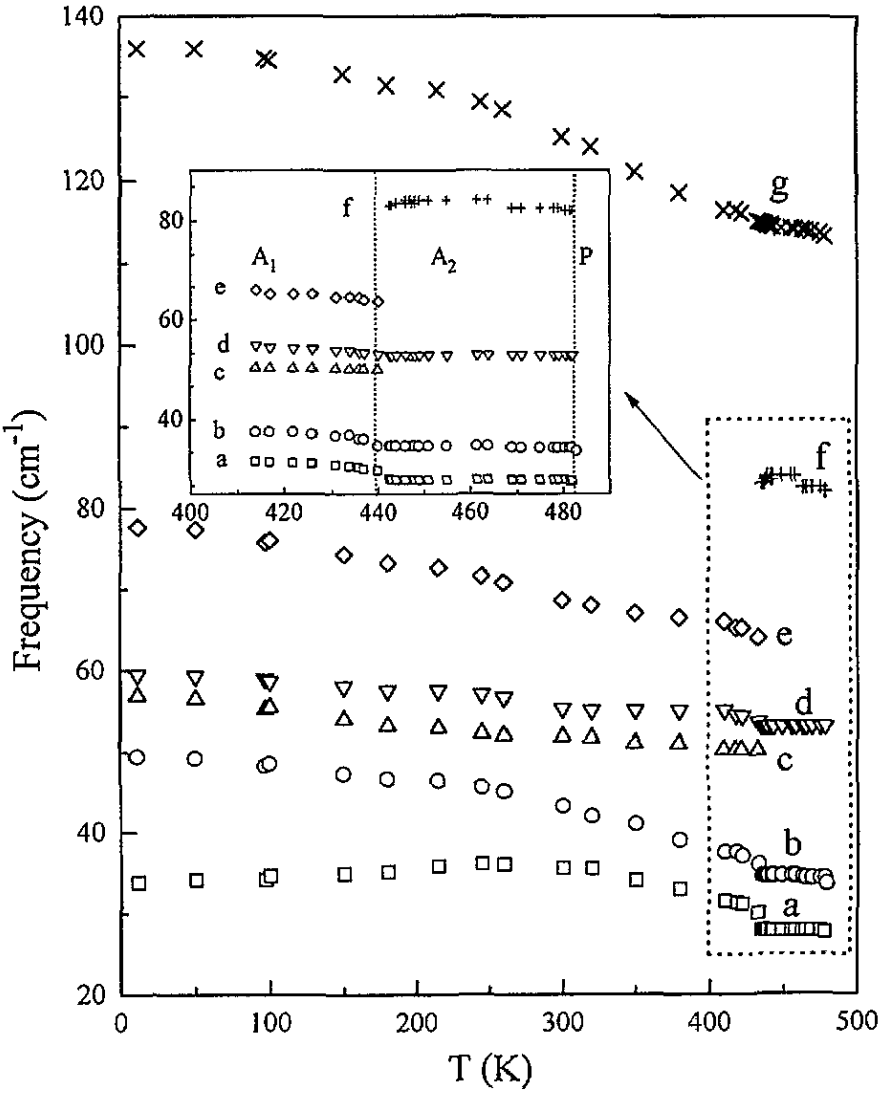

Figure 7. *Temperature dependence of Raman line frequencies throughout the whole* experimental temperature range for pure PH. The vicinity of the phase transitions is shown magnified in the inset.

to be antiferroelectric (using the Sawer–Tower system we observed double-hysteresis loops clearly in both phases), the question of the origin of this dielectric jump is open. From figure 8, reporting the quasi-elastic light scattering intensity as a function of temperature, no high-frequency relaxation process seems to occur at this $A_1 \rightarrow A_2$ phase transition. On the other hand, relative modifications in the phonon mode characteristics are noted in figures 7 and 10, especially for the lowest-frquency a and b modes.

For this reason we attempted to relate the dielectric jump to the anomaly of the a and b peaks at the phase transition and used the Lyddane–Sachs–Teller (LST) equation. We assumed that, except for the a and b modes considered as TO modes, all the other TO and LO modes are temperature independent. Consequently this modes contribute to the LST relation

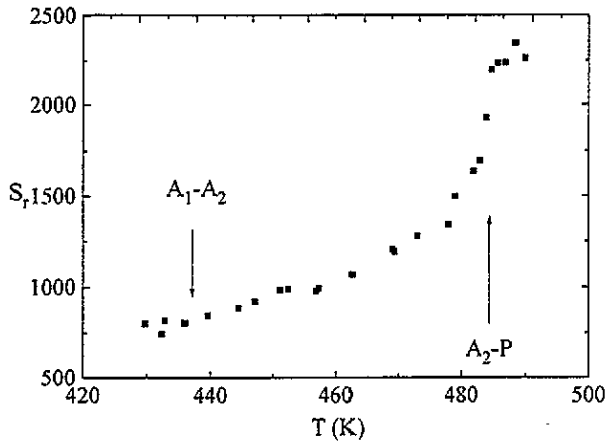

Figure 8. Temperature dependence of quasi-elastic scattering intensity for PH (on heating).

as a global constant, and only the modified a and b play a role in $\epsilon(0)$ jump. In both pure and Ti-doped samples, the downward jump of $\epsilon(0)$ from 600 in A_2 to 200 in A_1, can be described by the increase in frequency of the two a and b modes through this phase transition, all other contributions being considered as constant.

The results, presented in figure 11(a) for pure PH and 11(b) for PHT, give rather good and surprising agreement with the detected dielectric data.

Of course we are conscious that this calculation takes into account a strong assumption. Indeed, in the low-temperature phase A_1, all the modes measured by Raman scattering are *g* modes; consequently they are non-polar and do not participate in the dielectric properties. In the A_2 phase, this objection is removed. In fact, our assumption means that non-active Raman modes of *ungerade* symmetry (predicted by theory as infrared modes which are polar modes) are lying at equivalent frequencies to the visible a and b *gerade* modes. Furthermore all the other modes are stable through the transition. Since only about 40 modes are visible in the Raman spectra (instead of 48) and since no additional mode anomaly contributes to the jump appearing in the $A_1 \rightarrow A_2$ phase transition, such an assumption can find some justification.

3.4. Study of the $A_2 \rightarrow P$ transition and the scattering in the P phase for PH

As a continutation of figure 4, which showed the Raman spectra through the $A_2 \rightarrow$ P phase transition, in figure 12 we represent the Raman intensity temperature dependence above T_{A_2-P}. Since the paraelectric phase is from symmetrical considerations described by the $Pm3m$ space group, there should be no Raman-active mode in this phase. Our spectra exhibit, together with strong quasi-elastic diffusion (observed in figure 4) the strength of which has already been reported in figure 8, a broad shoulder whose intensity is found to be temperature dependent. Above T_{A_2-P} the global light scattering intensity still increases up to 525 K, then decreases and finally vanishes near 700 K.

The Raman scattering response has been fitted with a scattering function involving Debye-like quasi-elastic scattering and a highly overdamped phonon resonator. The results of such a fit are shown as an inset in figure 12.

The appearance of strong quasi-elastic scattering around T_{A_2-P} and its persistence above the transition temperature are known to be common features in many lead perovskite compounds [9, 21] and seem to indicate that this phase transition involves either strong

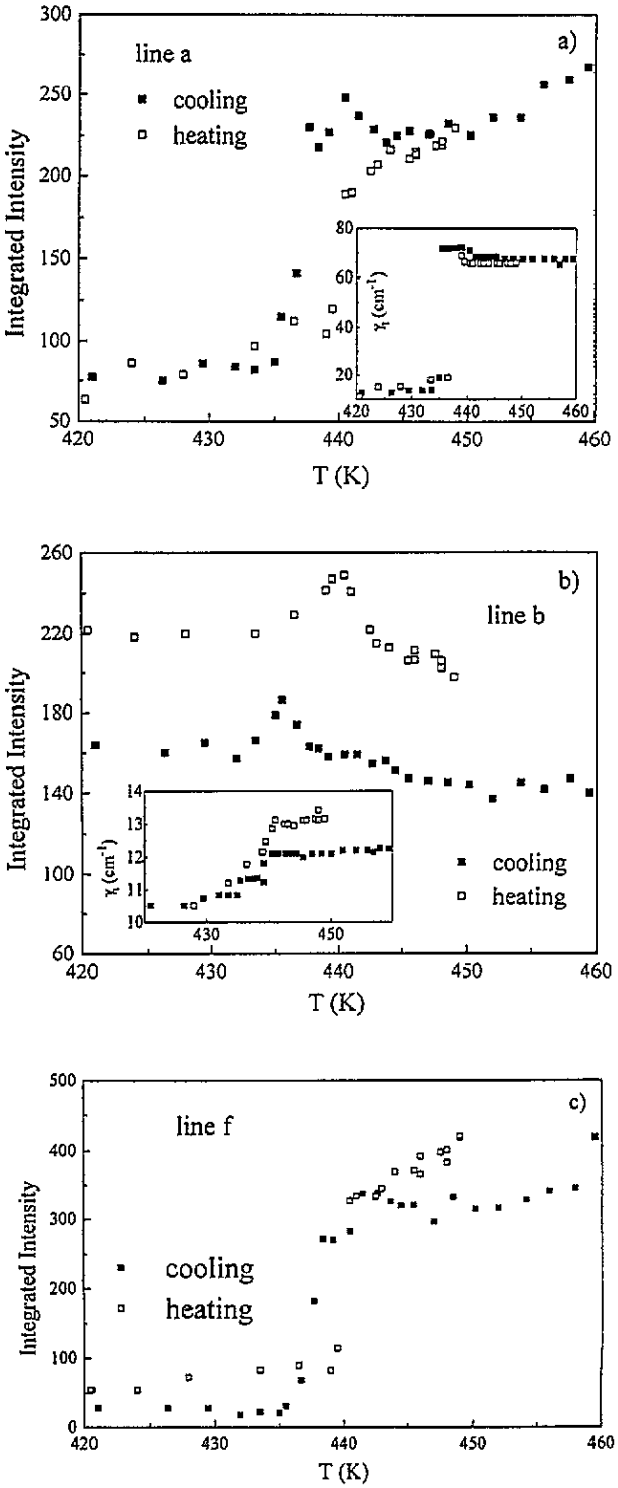

Figure 9. Temperature dependence of the calculated integrated intensity and half-width (inset) for (a) line a, (b) line b and (c) a new line f in the vicinity of the $A_1 \rightarrow A_2$ phase transition.

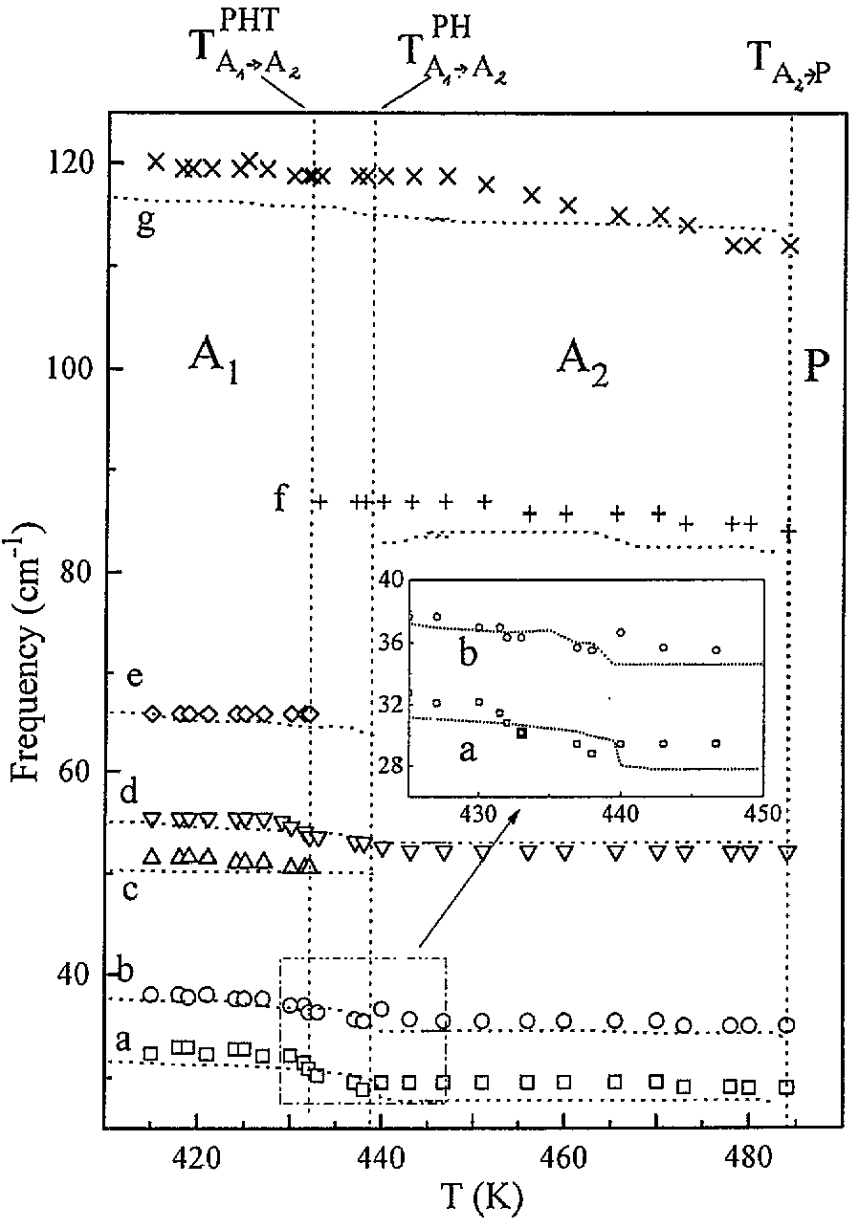

Figure 10. Temperature dependence of the Raman line frequencies from 400 to 480 K for PHT. The broken lines, added for comparison, show the corresponding frequencies obtained for a pure PH sample.

relaxational motion which is persistent even above T_c or the existence of some kind of disorder (static or dynamic). Disorder of this kind in the Pb sublattice, already reported in x-ray diffraction studies by Kwapulinski *et al* [22], has been shown to vanish near 700 K (as in our case).

This disorder could explain the activation of the lowest-frequency phonon modes (or a

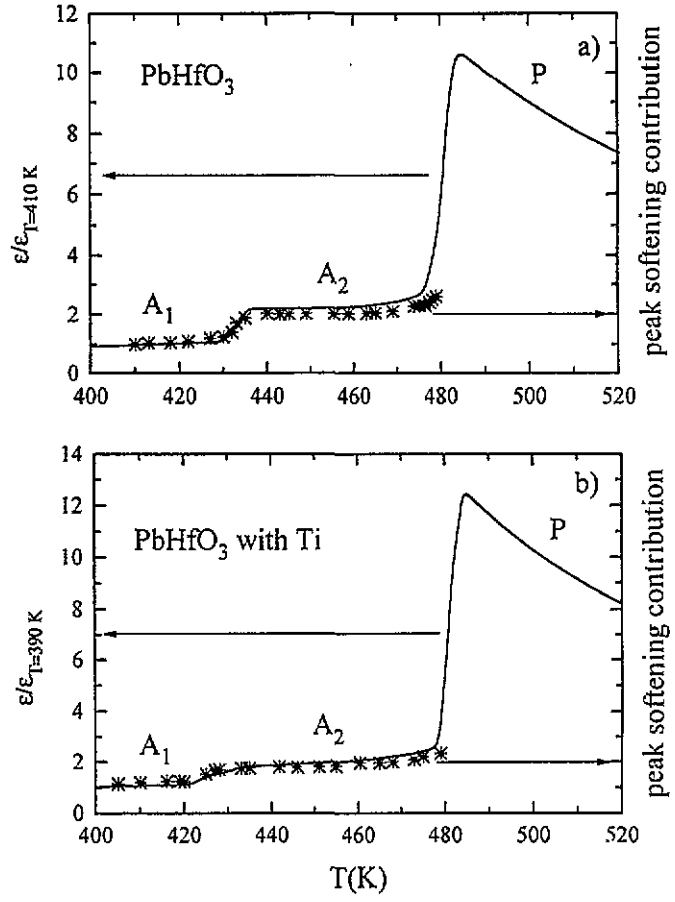

Figure 11. Comparison of the experimental dielectric permittivity as a function of temperature (——) with the calculated values from the LST relation (*) in the vicinity of the $A_1 \leftrightarrow A_2$ and $A_2 \leftrightarrow P$ phase transtions: (a) for a pure PH crystal; (b) for a PHT crystal.

phonon density of states) which is shown in our case as a broad shoulder. As deduced from our fit in the P phase this band gradually disappears with the disappearance of disorder and exhibits a frequency which is located in the energy range where the lowest-frequency mode appears in lead perovskites; furthermore significant softening is observed when approaching T_{P-A_2} (inset in figure 12).

4. Conclusions

The most important conclusion which can be drawn from the measurements presented here is that, in $PbHfO_3$ crystals, two phase transitions of quite different natures exist. The first, between two antiferroelectric phases, demonstrates a clear softening of the two low-frequency lines. This softening can be used to explain the radio-frequency $\epsilon'(T)$ behaviour at the $A_1 \rightarrow A_2$ phase transition. Since no change in the quasi-elastic scattering near this phase transition can be observed, hence this phase transition may be described as of displacive nature. The partial displacement of Hf ions by Ti does not change the nature

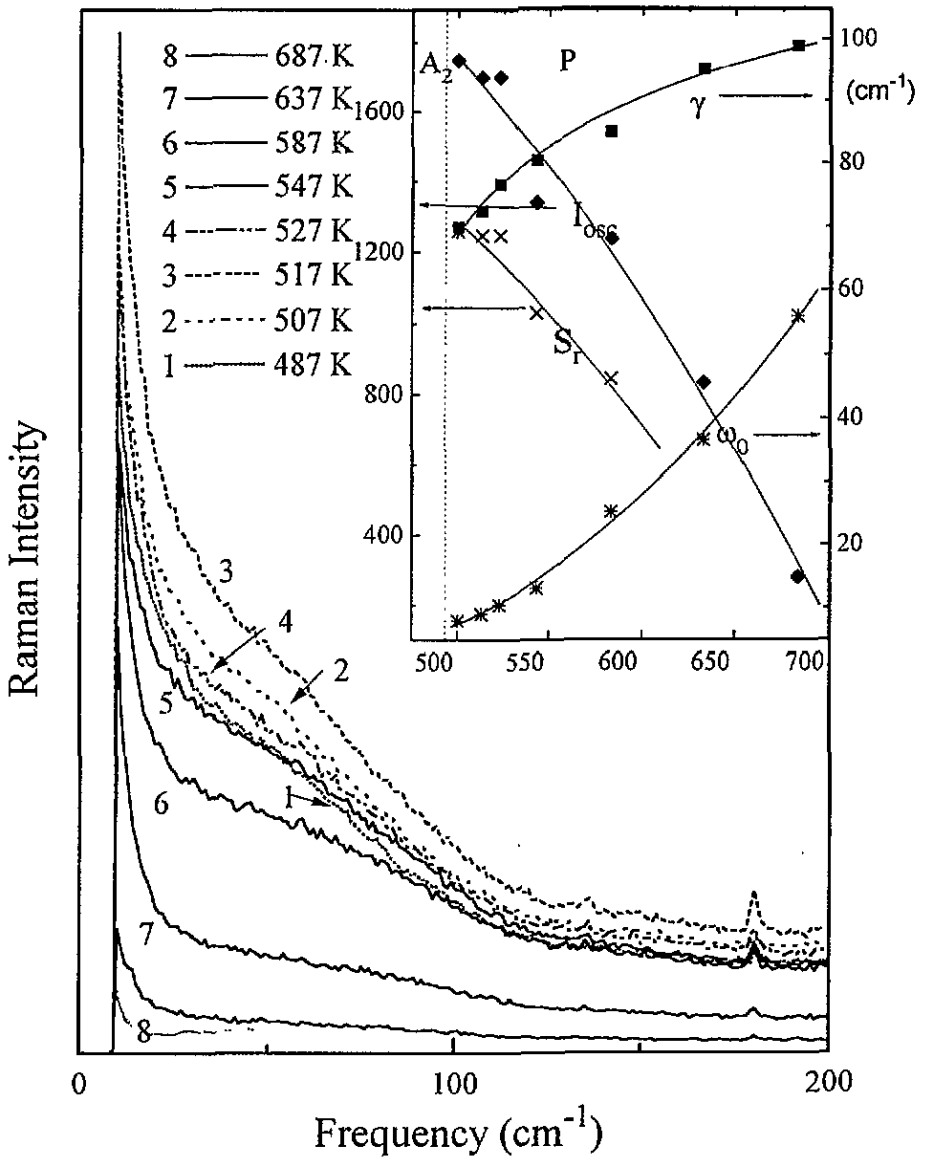

Figure 12. Raman spectra recorded for pure PH for various temperatures in the paraelectric phase. The results of a fit using a response function including an oscillator (ω_0, γ, I_{osc}) and a relaxor (of strength S_r) are shown in the inset.

of the $A_1 \rightarrow A_2$ phase transition but only widens the intermediate phase and leads to a smoother transition. The substitution of heavy Hf by much lighter Ti ions slightly shifts the positions of the lines a, f and g by a few reciprocal centimetres to higher frequencies, which proves that these modes involve the motion of B ions.

On the other hand, Ti doping does not affect the second $A_2 \rightarrow P$ phase transition and Raman spectra above T_c. Interpretation of the nature of this phase transition is much more complicated. According to the literature data the permittivity maximum at T_c may originate from a relaxational mode or from softening of a low-frequency optic mode, or from both.

It is worth recalling that a clear soft mode in antiferroelectric materials has not been found up to now in materials exhibiting a transition to an antiferroelectric phase. This is also the case, as indicated by data presented in this study, for PH and PHT. This means that a relaxation mode usually linked with the order–disorder nature of phase transition may be taken to be responsible for the dielectric response at T_c in these materials.

The Raman broad-band independence of Ti ions above T_c and also its temperature dependence corresponding to the behaviour of the disorder in the Pb sublattice found in x-ray investigations [22] tend to support this supposition.

If the nature of the high-temperature phase transition has even a partial order–disorder nature, it would be necessary to complete the investigations of low-frequency dielectric dispersion measurements in the paraelectric phase. Some measurements have already been performed for an antiferroelectric $PbZrO_3$ crystal which is similar in structure [7]. The relaxation found in that crystal in the very-low-frequency range (below 1 MHz) was shown also to have a marked influence on the $\epsilon'(T)$ function in the paraelectric phase and on the value of ϵ'_{max} at T_c.

Acknowledgments

One of the authors (IJ-S) would like to acknowledge the hospitality of the CLOES Laboratory at the University of Metz where this research was performed and also financial support by the French Government under the French–Polish scientific cooperation agreement.

References

[1] Sawaguchi E 1953 *J. Phys. Soc. Japan* **8** 615
[2] Handerek J and Ujma Z 1977 *Acta Phys. Pol.* A **51** 87
[3] Whatmore R W, Clarke R and Glazer A M 1978 *J. Phys. C: Solid State Phys.* **11** 3089
[4] Roleder K 1980 *Acta Phys. Pol.* A **58** 623
[5] Roleder K 1988 *Ferroelectrics* **81** 1217
[6] Handerek J, Kwapulinski J, Pawelczyk M and Ujma Z 1985 *Phase Trans.* **6** 35
[7] Jankowska I, Roleder K and Dec J 1993 *Ferroelectrics* **150** 436
[8] Pasto A E and Condrate R A 1973 *J. Am. Ceram. Soc.* **56** 436
[9] Roleder K, Kugel G E, Handerek J, Fontana M D, Carabatos C, Hafid M and Kania A 1988 *Ferroelectrics* **80** 161
[10] Roleder K, Jankowska I and Dec J 1993 *Phase Trans.* **42** 241
[11] Goulpeau L 1966 *Fiz. Tverd. Tela* **8** 2469
[12] Samara G A 1966 *Phys. Rev.* B **1** 3777
[13] Shirane G and Pepinski R 1953 *Phys. Rev.* B **91** 912
[14] Forker M, Hammersfahr A, Lopez-Garcia A and Wolbeck B 1973 *Phys. Rev.* B **7** 1039
[15] Zaitsev S M, Zhavoronko G P, Tatarenko A A, Kuprianow M F, Filipiev V S and Fesenko G E 1979 *Kristallografia* **24** 826
[16] Leontiev N G, Kolesova R V, Eremkin V V, Fesenko O E and Smotriakow V G 1984 *Sov. Phys.–Crystallogr.* **29** 238
[17] Tanaka M, Saito R and Suzuki K 1982 *J. Phys. Soc. Japan* **51** 2635
[18] Glazer A M, Roleder K and Dec J 1993 *Acta Crystallogr.* B **49** 846
[19] Maglione M, Böhmer R, Loidl A and Höchli U T 1989 *Phys. Rev.* B **40** 11 441
[20] Fontana M D, Idrissi H and Wójcik K 1990 *Europhys. Lett.* **11** 419
[21] Roleder K, Kugel G E, Fontana M D, Hańderek J, Lahlou S and Carabatos-Nédelec C 1989 *J. Phys.: Condens. Matter* **1** 2257
[22] Kwapulinski J, Pawelczyk M and Dec J 1994 *J. Phys.: Condens. Matter* **6** 4655